

# Chapman-Enskog expansion for chirally colliding disks

Ruben Lier<sup>1,2,3,\*</sup> and Paweł Matus<sup>4</sup>

<sup>1</sup>*Institute for Theoretical Physics, University of Amsterdam, 1090 GL Amsterdam, The Netherlands*

<sup>2</sup>*Dutch Institute for Emergent Phenomena (DIEP),  
University of Amsterdam, 1090 GL Amsterdam, The Netherlands*

<sup>3</sup>*Institute for Advanced Study, University of Amsterdam,  
Oude Turfmarkt 147, 1012 GC Amsterdam, The Netherlands*

<sup>4</sup>*School of Physics and Astronomy, Tel Aviv University, Tel Aviv, Israel*

We study a two-dimensional fluid of hard disks undergoing chiral, energy- and momentum-conserving collisions. We show that despite the microscopic breaking of time-reversal symmetry, the  $H$ -theorem is obeyed, guaranteeing a relaxation towards equilibrium in the absence of external forces. In the dilute limit, a Chapman-Enskog expansion yields analytical expressions for the shear and odd viscosity and the thermal conductivity. Theoretical predictions are confirmed by nonequilibrium molecular dynamics simulations.

## I. INTRODUCTION

The kinetic theory of gases was built on the image of colliding billiard balls, identical and symmetric, their interactions governed only by geometry, conservation laws, and discrete symmetries. Although these microscopic encounters are reversible, an *arrow of time* emerges at macroscopic scales, breaking time-reversal symmetry. This breaking gives rise to dissipative transport such as shear viscosity, thermal conductivity, and the diffusivity of dyes.

In addition to time-reversal symmetry, another important discrete symmetry in kinetic theory is parity. In two dimensions, it is possible for parity and time-reversal symmetry to be simultaneously broken at the microscopic level, which happens when the system is *chiral*. One of the key transport implications from chirality in two dimensions is a nonvanishing *odd viscosity*, a mysterious transport coefficient that in two dimensions only affects the flow under specific circumstances [1–13]. In addition, chirality causes “odd thermal conductivity”, which is also called the Righi-Leduc effect [14]. For charged particles, there can be an odd charge conductivity, also called the Hall conductivity [15]. Chirality typically enters kinetic theory in one of the following two ways:

1. Chirality is introduced by turning on a magnetic field or Coriolis force felt by all the particles [16–23] (see Refs. [24–29] for kinetic theory treatments).
2. Chirality is introduced through an external torque acting on each particle [30–37] (see Refs. [38, 39] for kinetic theory treatments).

In this work, we take a different approach to chirality in kinetic theory. We consider a gas of hard disks [40–42] without explicitly introducing a background field or a microscopic driving mechanism. Instead, chirality

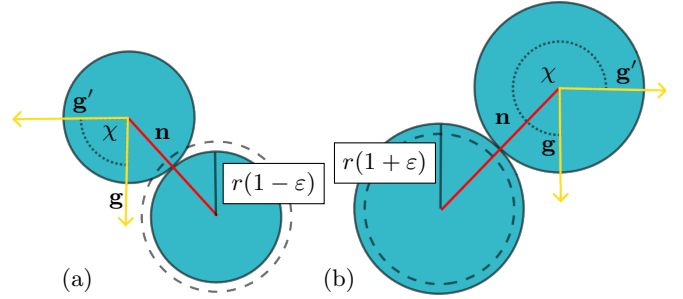


FIG. 1: Depiction of collision with chiral effective particle radii  $r(1 \pm \epsilon)$ .  $\mathbf{g}$  is the relative velocity,  $\mathbf{n}$  is the vector connecting the centers of the colliding objects,  $\mathbf{g}'$  is the outgoing relative velocity, and  $\chi$  is the scattering angle.

enters intrinsically at the particle level: particles discriminate between left- and right-handed encounters with other particles by biasing whether or not a collision takes place.

Crucially, this chiral property modifies only the rate of left- versus right-handed collisions, while leaving the hard-disk collision rule itself unchanged. As a result, energy, momentum, and angular momentum are all conserved, meaning that additional degrees of freedom like the particles’ orientation are not necessary for a consistent description. Furthermore, although these chiral collisions violate parity and time-reversal symmetry,  $H$ -theorem is found to be upheld, which means that a well-defined equilibrium state exists. With respect to this equilibrium state, we can expand the theory to obtain gradient corrections to the constitutive equations, allowing us to obtain first-order transport coefficients. In the dilute limit, this can be done with an exact method which is the Chapman-Enskog expansion [24]. The hard disk nature of the considered model makes it ideally suited for a simulation of nonequilibrium molecular dynamics (NEMD) which we use to numerically corroborate the results based on the Chapman-Enskog expansion.

\* r.liet@uva.nl

## II. THE MODEL

Let us now describe the model of chiral hard disks in full detail. We consider a gas of particles of mass  $m$ , whose collisions conserve energy and momentum. That is, when two particles with ingoing velocity  $\mathbf{v}_1$  and  $\mathbf{v}_2$  collide, the outgoing velocities  $\mathbf{v}'_1$  and  $\mathbf{v}'_2$  obey

$$\mathbf{v}_1 + \mathbf{v}_2 = \mathbf{v}'_1 + \mathbf{v}'_2, \quad (1a)$$

$$v_1^2 + v_2^2 = v_1'^2 + v_2'^2. \quad (1b)$$

After satisfying (1), the only thing that is left free is the orientation of the outgoing relative velocity with respect to the ingoing one, i.e.

$$\mathbf{g}' = \mathbf{R}(\chi) \cdot \mathbf{g}, \quad (2)$$

where  $\mathbf{g} = \mathbf{v}_2 - \mathbf{v}_1$  and  $\mathbf{g}' = \mathbf{v}'_2 - \mathbf{v}'_1$  are the relative velocities and  $\mathbf{R}(\chi)$  is the two-dimensional rotation matrix that depends only on the scattering angle  $\chi$ . Hard disk collisions occur instantly when two particles start to overlap. For perfectly smooth hard disks, the forces are exerted along the line of disk centers  $\mathbf{n}$ , and consequently angular momentum is conserved as well.

To introduce chirality without abandoning the simplicity of the hard disk model, we consider the following toy model. Based on the chirality of the collision  $c$ , which is given by

$$c = \text{sign}[\hat{\mathbf{z}} \cdot (\mathbf{n} \times \mathbf{g})], \quad (3)$$

we attribute a different *effective radius*  $r(1+c\epsilon)$  to colliding particles, see Fig. 1. Considering the geometry of a hard disk collision, one finds that the impact parameter  $b$  and the scattering angle  $\chi$  are related through

$$\begin{aligned} b &= d(1 + \epsilon) \sin(\chi/2), & b > 0, \\ b &= d(1 - \epsilon) \sin(\chi/2), & b < 0, \end{aligned} \quad (4)$$

where  $d = 2r$  is the average diameter. Because the chirality only affects when the particles collide but not the collision rule itself, the model automatically upholds all conservation laws and furthermore ensures the validity of the  $H$ -theorem, making it possible to perform a local equilibrium expansion by means of Chapman-Enskog procedure.

The concept of the chirality  $c$  of a collision was used in Ref. [43] to model ratchets in a dense suspension. There, the ratchets were modelled as hard disks that are perfectly smooth or infinitely rough depending on chirality  $c$ , which allowed the authors of Ref. [43] to numerically obtain a nonvanishing odd viscosity. Here, in order to illustrate how our toy model compares with a particular realization of a chirally colliding gas, we consider collisions of ratchet-shaped particles such as shown in Fig. 2. As described in App. A, we perform a numerical collision experiment, where we consider an ensemble of particles with velocities  $\mathbf{v}$  and angular velocities  $\omega$  which follow the biased Maxwell-Boltzmann distribution

$$f_{\text{MB}}(\omega, \mathbf{v}) \sim \exp\left(-\frac{m\mathbf{v}^2 + I(\omega - \Omega)^2}{2k_b T}\right), \quad (5)$$

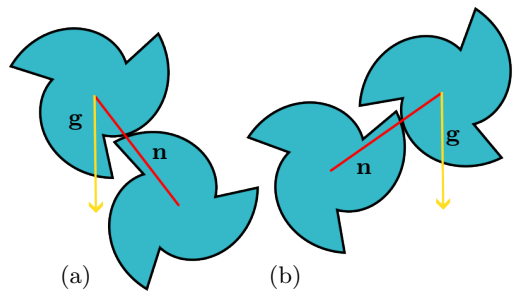


FIG. 2: Schematic picture of two ratchet-shaped particles moving towards each other in two chirally distinct ways.

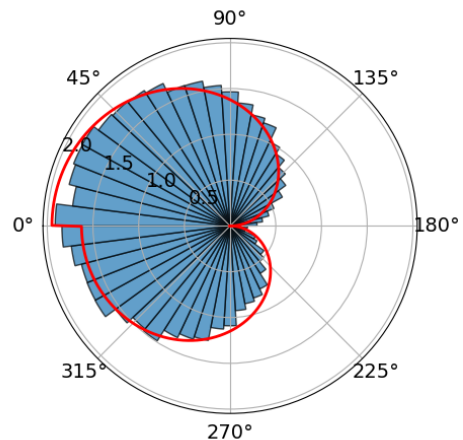


FIG. 3: Scattering cross section as a function of scattering angle  $\chi$  corresponding to the numerical collision experiment of ratchet-shaped particles (see Fig. 2). The particles follow the biased Maxwell-Boltzmann statistic of Eq. (5) with

$\Omega = 0.2\sqrt{2k_b T/I}$ . The red line corresponds to the corresponding scattering cross section for the collision rule with chiral effective radii (see Fig. 1), where we fitted  $r = 1.79$  and  $\epsilon = 0.09$ . For more details see App. A.

where  $m$  is the particle's mass,  $I$  is the moment of inertia,  $T$  is the temperature, and  $\Omega$  is the average rotation frequency. We let these particles collide at all impact parameters, keeping track of the scattering angle  $\chi$ . The corresponding histogram of scattering angles is shown in Fig. 3. Due to the interplay of the chiral shape and a nonzero average rotation, the histogram displays a chiral shape, which can potentially lead to chiral transport.

Having specified the nature of the chiral collisions, we can formulate the Boltzmann equation which describes the evolution of the phase-space distribution  $f(\mathbf{v}, \mathbf{x}, t)$  of the disks in the dilute limit. The Boltzmann equation is

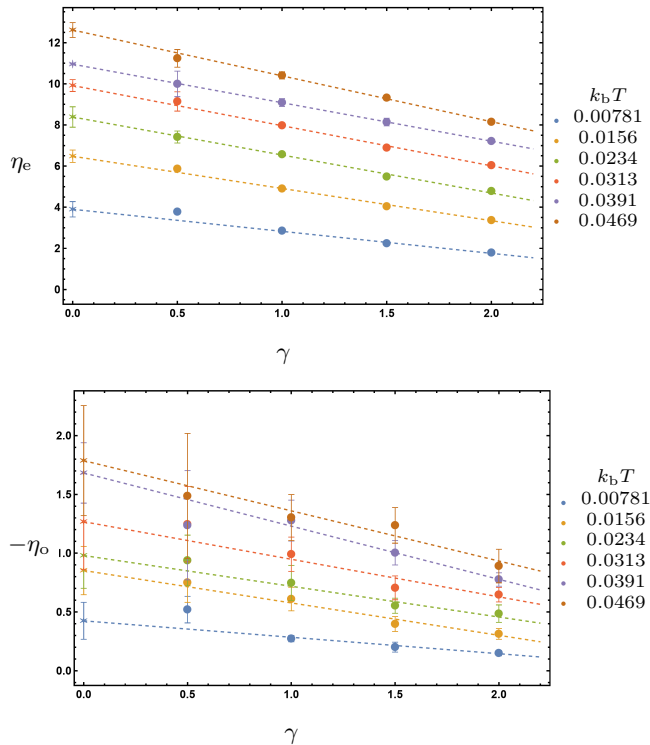


FIG. 4: Extrapolation of numerically obtained shear viscosity  $\eta_e$  (top) and odd viscosity  $\eta_o$  (bottom) to infinitesimal shear rate  $\gamma$  for  $\varepsilon = 0.5$ .

given by

$$\mathcal{L}[f(\mathbf{v}_1)] = C[f(\mathbf{v}_1)]. \quad (6)$$

The left-hand side of the Boltzmann equation (6) is called the streaming term, while the right-hand side is called the collision term. For the type of hard disks considered in this work, these terms are given by

$$\mathcal{L}[f(\mathbf{v}_1)] = \partial_t f(\mathbf{v}_1) + \mathbf{v}_1 \cdot \nabla f(\mathbf{v}_1) \quad , \quad (7a)$$

$$C[f(\mathbf{v}_1)] = \int d\mathbf{v}_2 \int_{d(1-\varepsilon)}^{d(1+\varepsilon)} db |\mathbf{g}| (f(\mathbf{v}'_1) f(\mathbf{v}'_2) - f(\mathbf{v}_1) f(\mathbf{v}_2)), \quad (7b)$$

where we omitted the dependence of the phase-space distribution on  $t$  and  $\mathbf{x}$  for simplicity. Following Eq. (4),

$$C^{(1)}[\Phi](\mathbf{v}_1) = - \int d\mathbf{v}_2 f_0(\mathbf{v}_2) \sum_{\pm} \pm \frac{d(1 \pm \varepsilon)}{2} \int_0^{\pm\pi} d\chi \sin(\chi/2) |\mathbf{g}| [\Phi(\mathbf{v}_1) + \Phi(\mathbf{v}_2) - \Phi(\mathbf{v}'_1) - \Phi(\mathbf{v}'_2)]. \quad (12)$$

In the equation above we dropped the arguments  $\mathbf{x}$  and  $t$  since they are equal for all the functions. Calculating

Eq. (7b) can be written as

$$C[f(\mathbf{v}_1)] = \int d\mathbf{v}_2 \sum_{\pm} \pm \frac{d(1 \pm \varepsilon)}{2} \int_0^{\pm\pi} d\chi \cdot \sin(\chi/2) |\mathbf{g}| (f(\mathbf{v}'_1) f(\mathbf{v}'_2) - f(\mathbf{v}_1) f(\mathbf{v}_2)). \quad (8)$$

### III. CHAPMAN-ENSKOG EXPANSION

Due to their chiral nature, the collisions described in Sec. II break both parity and time reversal – two symmetries commonly assumed in the derivation of the  $H$ -theorem [44, 45]. What is more, the collision rules in our toy model do not follow from any Hamiltonian. Nevertheless, as long as the collisions conserve energy and momentum, the  $H$ -theorem must hold, as we rigorously prove in App. B. Therefore, the system possesses a well-defined thermal equilibrium in which the particles obey the Maxwell-Boltzmann distribution. This observation forms the foundation of the hydrodynamic approach to transport. The system is assumed to be in the vicinity of a *local* equilibrium state described by the distribution function

$$f_0(\mathbf{v}, \mathbf{x}, t) = \frac{n(\mathbf{x}, t)}{2\pi k_b T(\mathbf{x}, t)} \exp\left(-\frac{m(\mathbf{v} - \mathbf{u}(\mathbf{x}, t))^2}{2k_b T(\mathbf{x}, t)}\right). \quad (9)$$

Here, velocity  $\mathbf{u}(\mathbf{x}, t)$ , disk density  $n(\mathbf{x}, t)$ , and temperature  $T(\mathbf{x}, t)$  are functions of time and space and are assumed to vary slowly in comparison to the typical relaxation time and the mean free path for collisions. Importantly, any distribution function of the form (9) is a solution of the collisional part of the Boltzmann equation:  $\mathcal{C}[f_0] = 0$ , but the corresponding streaming term is generically nonzero:  $\mathcal{L}[f_0] \neq 0$ . The Chapman-Enskog expansion assumes that the actual solution to the Boltzmann equation can be approximated by a series of perturbations to  $f_0(\mathbf{v}, \mathbf{x}, t)$ :

$$f(\mathbf{v}, \mathbf{x}, t) = f_0(\mathbf{v}, \mathbf{x}, t) [1 + \Phi(\mathbf{v}, \mathbf{x}, t) + \dots], \quad (10)$$

where each successive term is proportional to higher gradients of  $\mathbf{u}(\mathbf{x}, t)$  and  $T(\mathbf{x}, t)$ . The first-order correction  $\Phi(\mathbf{v}, \mathbf{x}, t)$  is found by solving the equation

$$\mathcal{L}[f_0] = f_0 C^{(1)}[\Phi], \quad (11)$$

where the right-hand side is the collision term  $\mathcal{C}[f_0(1+\Phi)]$  expanded to the linear order in  $\Phi(\mathbf{v}, \mathbf{x}, t)$ :

the transport coefficients from (11) using the Chapman-

Enskog theory involves a truncated expansion of  $\Phi$  in Sonine polynomials, which is worked out in App. C. We find the following viscosities  $\eta_{e,o}$  and thermal conductivities  $\kappa_{e,o}$  for a Sonine expansion truncated at order  $N$ :

$$\begin{aligned}\eta_e^{(N)} &= \eta_e^{(0)} N_e^{(N)}(\varepsilon), & \eta_o^{(N)} &= \eta_o^{(0)} N_o^{(N)}(\varepsilon), \\ \kappa_e^{(N)} &= \kappa_e^{(0)} K_e^{(N)}(\varepsilon), & \kappa_o^{(N)} &= \kappa_o^{(0)} K_o^{(N)}(\varepsilon),\end{aligned}\quad (13)$$

where the transport coefficients at zeroth order in a Sonine polynomial expansion are given by

$$\begin{aligned}\eta_e^{(0)} &= \frac{8}{d(16 + \varepsilon^2)} \sqrt{\frac{mk_b T}{\pi}}, & \eta_o^{(0)} &= -\frac{2\varepsilon}{d(16 + \varepsilon^2)} \sqrt{\frac{mk_b T}{\pi}}, \\ \kappa_e^{(0)} &= \frac{32k_b T}{d(16 + \varepsilon^2)} \sqrt{\frac{k_b T}{\pi m}}, & \kappa_o^{(0)} &= -\frac{8\varepsilon k_b T}{d(16 + \varepsilon^2)} \sqrt{\frac{k_b T}{\pi m}},\end{aligned}\quad (14)$$

whereas the functions  $N_{e,o}^{(N)}(\varepsilon)$  and  $K_{e,o}^{(N)}(\varepsilon)$  are multiplicative corrections corresponding to the order at which the Sonine polynomial expansion is truncated. Taking  $N = 5$  and  $\varepsilon = 0.5$ , we find

$$\begin{aligned}N_e^{(5)}(0.5) &= 1.02196, & N_o^{(5)}(0.5) &= 1.02166, \\ K_e^{(5)}(0.5) &= 1.02994, & K_o^{(5)}(0.5) &= 1.02002.\end{aligned}\quad (15)$$

Since these multiplicative correction coefficients are close to one, the truncation error can be assumed to be small.

To verify (14), we use nonequilibrium molecular dynamics. In particular, we consider a shear periodic box of hard disks which collide with the collision rule of (1). We turn on shear with the SLLOD algorithm [34, 46–48]. The details of this simulation are provided in App. D and the full code and simulation output is available at <https://github.com/rubenlier/chiral-chapman-enskog>. When implementing the SLLOD algorithm, one faces a tradeoff, where increasing the shear rate  $\gamma$  on the one hand accelerates convergence of the result, and on the other hand introduces nonlinear corrections related to shear thinning [49]. For this reason, to get rid of this systematic error, we compute the shear and odd viscosity at different values of shear rate and extrapolate to the regime where shear rate is infinitesimal (see Fig. 4). The resulting shear and odd viscosities are given in Fig. 5.

We see in Fig. 5 that the overlap between numerical results and the theory is strong, although we also observe some systematic downward bias at low temperatures and, in the case of odd viscosity, an upward bias at high temperatures. Furthermore, the relative statistical error of odd viscosity is much higher, which is explained by that, as follows from (14), the odd viscosity considered in this work is always one order of magnitude smaller than shear viscosity, which strongly lowers the signal-to-noise ratio. We explain the downward discrepancy at low temperatures by a strongly nonlinear dependence of the measured viscosity on the shear rate  $\gamma$ , which can be seen for a small

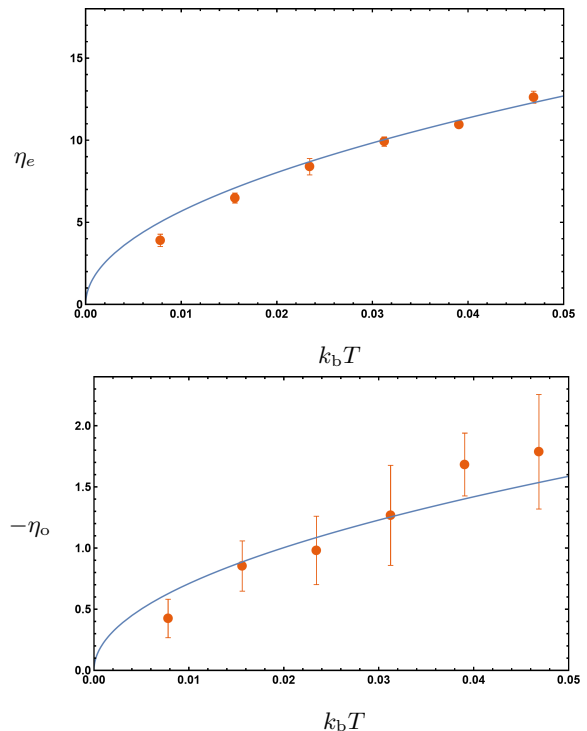


FIG. 5: Shear viscosity  $\eta_e$  (top) and odd viscosity  $\eta_o$  (bottom) as a function of  $k_b T$  for  $\varepsilon = 0.5$ . The numerical results were obtained using the extrapolation shown in Fig. 4.

$\gamma$  in Fig. 4, and which leads to an underestimation of the true result. In fact, if the dependence of  $\eta_e$  on  $\gamma$  were strictly linear, the measured  $\eta_e$  would become negative for a large enough  $\gamma$ , which is unphysical. Regarding the upward trend for the odd viscosity at high temperatures, we notice that the length scale associated with a nonvanishing odd viscosity is given by  $d\varepsilon$ , whereas for shear viscosity this is  $d$ , so that odd viscosity is more sensitive to finite resolution effects which become more important when temperature is increased.

#### IV. DISCUSSION

In this work, we introduce a new microscopic approach to odd viscosity, which relies neither on a background parity-odd field nor on the external inflow of angular momentum. Instead, the approach is based on hard disks with chiral effective radii. Because the collision rule obeys particle number, energy, and momentum conservation, it is possible to find the equilibrium state, with respect to which we expand to compute parity-even and parity-odd transport. The resulting expressions for viscosity are compared to a computation of viscosity using nonequilibrium molecular dynamics simulations. This work is the first one we are aware of where odd viscosity is calculated from first principles and coincides with the

result of a many-particle simulation.

## V. ACKNOWLEDGEMENTS

We thank Tobias Holder, Tomer Markovich, Naomi Oppenheimer and Jan V. Sengers for useful discussions. P.M. was supported by the European Research Council (ERC) under grant QuantumCUSP (Grant Agreement No. 101077020), the Harry Bloomfield International Scholarship, and a postdoctoral fellowship of the Azrieli foundation.

- 
- [1] Carlos Hoyos and Dam Thanh Son. Hall viscosity and electromagnetic response. *Physical Review Letters*, 108(6), February 2012.
- [2] Luca V. Delacrétaz and Andrey Gromov. Transport Signatures of the Hall Viscosity. *Phys. Rev. Lett.*, 119(22):226602, 2017.
- [3] Sriram Ganeshan and Alexander G. Abanov. Odd viscosity in two-dimensional incompressible fluids. *Phys. Rev. Fluids*, 2(9):094101, 2017.
- [4] J. E. Avron. Odd Viscosity. *J. Stat. Phys.*, 92(3/4):543–557, 1998.
- [5] Ruben Lier. Slip-induced odd viscous flow past a cylinder. *Phys. Rev. Fluids*, 9:094101, Sep 2024.
- [6] Ruben Lier, Charlie Duclut, Stefano Bo, Jay Armas, Frank Jülicher, and Piotr Surówka. Lift force in odd compressible fluids. *Phys. Rev. E*, 108:L023101, Aug 2023.
- [7] Yuto Hosaka, Shigeyuki Komura, and David Andelman. Hydrodynamic lift of a two-dimensional liquid domain with odd viscosity. *Phys. Rev. E*, 104(6):064613, 2021.
- [8] Yuto Hosaka, Shigeyuki Komura, and David Andelman. Nonreciprocal response of a two-dimensional fluid with odd viscosity. *Phys. Rev. E*, 103(4):042610, 2021.
- [9] Abdallah Daddi-Moussa-Ider, Andrej Vilfan, and Yuto Hosaka. Analytical solution for the hydrodynamic resistance of a disk in a compressible fluid layer with odd viscosity on a rigid substrate. *The Journal of Chemical Physics*, 162(6):064103, 02 2025.
- [10] Andrew Lucas and Piotr Surówka. Phenomenology of nonrelativistic parity-violating hydrodynamics in 2+1 dimensions. *Physical Review E*, 90(6), December 2014.
- [11] Alexander Abanov, Tankut Can, and Sriram Ganeshan. Odd surface waves in two-dimensional incompressible fluids. *SciPost Phys.*, 5(1):010, 2018.
- [12] Jarosław Pawłowski, Marcin Dudziak, Matteo Baggioli, Jie Zhang, and Piotr Surówka. Lift force in chiral, compressible granular matter. *Phys. Rev. E*, 112:055423, Nov 2025.
- [13] I. V. Gornyi and D. G. Polyakov. Two-dimensional electron hydrodynamics in a random array of impenetrable obstacles: Magnetoresistivity, hall viscosity, and the landauer dipole. *Phys. Rev. B*, 108:165429, Oct 2023.
- [14] A. Leduc. Modifications de la conductibilité calorifique du bismuth dans un champ magnétique. *Journal de Physique Théorique et Appliquée*, 7(1):519–525, 1888.
- [15] E. H. Hall. On a new action of the magnet on electric currents. *American Journal of Mathematics*, 2(3):287, September 1879.
- [16] Francesco M. D. Pellegrino, Iacopo Torre, and Marco Polini. Nonlocal transport and the Hall viscosity of two-dimensional hydrodynamic electron liquids. *Phys. Rev. B*, 96(19):195401, 2017.
- [17] A. I. Berdyugin, S. G. Xu, F. M. D. Pellegrino, R. Krishna Kumar, A. Principi, I. Torre, M. Ben Shalom, T. Taniguchi, K. Watanabe, I. V. Grigorieva, M. Polini, A. K. Geim, and D. A. Bandurin. Measuring Hall viscosity of graphene’s electron fluid. *Science*, 364(6436):162–165, 2019.
- [18] H. Hulsmans, E.J. Van Waasdijk, A.L.J. Burgmans, H.F.P. Knaap, and J.J.M. Beenakker. Transverse momentum transport in polyatomic gases under the influence of a magnetic field. *Physica*, 50(1):53–76, 1970.
- [19] P. S. Alekseev. Negative magnetoresistance in viscous flow of two-dimensional electrons. *Phys. Rev. Lett.*, 117:166601, Oct 2016.
- [20] J. Korving, H. Hulsmans, H.F.P. Knaap, and J.J.M. Beenakker. Transverse momentum transport in viscous flow of diatomic gases in a magnetic field. *Physics Letters*, 21(1):5–7, April 1966.
- [21] P eter L evay. Berry phases for Landau Hamiltonians on deformed tori. *J. Math. Phys.*, 36(6):2792–2802, 1995.
- [22] J. E. Avron, R. Seiler, and P. G. Zograf. Viscosity of Quantum Hall Fluids. *Phys. Rev. Lett.*, 75(4):697–700, 1995.
- [23] Carlos Hoyos. Hall viscosity, topological states and effective theories. *International Journal of Modern Physics B*, 28(15):1430007, 2014.
- [24] S. Chapman and T.G. Cowling. *The Mathematical Theory of Non-uniform Gases: An Account of the Kinetic Theory of Viscosity, Thermal Conduction and Diffusion in Gases*. Cambridge Mathematical Library. Cambridge University Press, 1990.
- [25] Paweł Matus, Rajesh Biswas, Piotr Surówka, and Francisco Pe na-Ben itez. Non-relativistic transport from frame-indifferent kinetic theory, 2024.
- [26] L P Pitaevskii, E M Lifshitz, and A M Kosevich. *Physical Kinetics*. Butterworth-Heinemann, Oxford, England, November 1981.
- [27] Yu. Kagan and L. Maksimov. Transport phenomena in a paramagnetic gas. *Soviet Physics JETP*, 14(3):842–852, March 1962.
- [28] H.F.P. Knaap and J.J.M. Beenakker. Heat conductivity and viscosity of a gas of non-spherical molecules in a magnetic field. *Physica*, 33(3):643–670, 1967.
- [29] H. Moraal, F.R. McCourt, and Knaap H.F.P. The Senftleben-Beenakker effects for a gas of rough spherical molecules: II. the viscosity scheme. *Physica*, 45(3):455–468, 1969.

- [30] Vishal Soni, Ephraim S. Bililign, Sofia Magkiriadou, Stefano Sacanna, Denis Bartolo, Michael J. Shelley, and William T. M. Irvine. The odd free surface flows of a colloidal chiral fluid. *Nat. Phys.*, 15:1188–1194, 2019.
- [31] Tomer Markovich and Tom C. Lubensky. Nonreciprocity and odd viscosity in chiral active fluids. *Proceedings of the National Academy of Sciences*, 121(19):e2219385121, 2024.
- [32] Cory Hargus, Katherine Klymko, Jeffrey M. Epstein, and Kranthi K. Mandadapu. Time reversal symmetry breaking and odd viscosity in active fluids: Green–Kubo and NEMD results. *J. Chem. Phys.*, 152(20):201102, 2020.
- [33] Cory Hargus, Jeffrey M. Epstein, and Kranthi K. Mandadapu. Odd Diffusivity of Chiral Random Motion. *Phys. Rev. Lett.*, 127(17):178001, 2021.
- [34] Ming Han, Michel Fruchart, Colin Scheibner, Suriyanarayanan Vaikuntanathan, Juan J. de Pablo, and Vincenzo Vitelli. Fluctuating hydrodynamics of chiral active fluids. *Nat. Phys.*, 17(11):1260, 2021.
- [35] Anthony R. Poggioli and David T. Limmer. Odd mobility of a passive tracer in a chiral active fluid. *Phys. Rev. Lett.*, 130:158201, Apr 2023.
- [36] Paweł Matus, Ruben Lier, and Piotr Surówka. Molecular modelling of odd viscoelastic fluids, 2024.
- [37] Debarghya Banerjee, Anton Souslov, Alexander G. Abanov, and Vincenzo Vitelli. Odd viscosity in chiral active fluids. *Nat. Commun.*, 8(1):1573, 2017.
- [38] Ege Eren, Michel Fruchart, and Vincenzo Vitelli. A collisional model of odd fluids: from boltzmann equation to chiral hydrodynamics, 2025.
- [39] Michel Fruchart, Ming Han, Colin Scheibner, and Vincenzo Vitelli. The odd ideal gas: Hall viscosity and thermal conductivity from non-Hermitian kinetic theory. [arXiv:2202.02037](https://arxiv.org/abs/2202.02037), 2022.
- [40] David M. Gass. Enskog theory for a rigid disk fluid. *The Journal of Chemical Physics*, 54(5):1898–1902, 03 1971.
- [41] J. V. Sengers. Divergence in the density expansion of the transport coefficients of a two-dimensional gas. *The Physics of Fluids*, 9(9):1685–1696, 09 1966.
- [42] B. J. Alder and T. E. Wainwright. Phase transition in elastic disks. *Phys. Rev.*, 127:359–361, Jul 1962.
- [43] Zhiyuan Zhao, Mingcheng Yang, Shigeyuki Komura, and Ryohei Seto. Odd viscosity in chiral passive suspensions. *Frontiers in Physics*, 10, October 2022.
- [44] S.R. De Groot and P. Mazur. *Non-Equilibrium Thermodynamics*. Dover Publications, New York, U.S.A., 1984.
- [45] Carlo Cercignani. *The Boltzmann Equation and Its Applications*. Springer New York, 1988.
- [46] Denis J Evans and Gary Morriss. *Statistical mechanics of nonequilibrium liquids*. ANU Press, Canberra, Australia, August 2007.
- [47] Denis J. Evans and G. P. Morriss. Nonlinear-response theory for steady planar couette flow. *Phys. Rev. A*, 30:1528–1530, Sep 1984.
- [48] Peter J. Daivis and B. D. Todd. A simple, direct derivation and proof of the validity of the slod equations of motion for generalized homogeneous flows. *The Journal of Chemical Physics*, 124(19):194103, 05 2006.
- [49] Evan Evans and Erich Sackmann. Translational and rotational drag coefficients for a disk moving in a liquid membrane associated with a rigid substrate. *J. Fluid Mech.*, 194(-1):553, 1988.
- [50] Ludwig Boltzmann. *Lectures on Gas Theory*. University of California Press, December 1964.
- [51] Carlo Cercignani and Maria Lampis. On the H-theorem for polyatomic gases. *Journal of Statistical Physics*, 26(4):795–801, Dec 1981.
- [52] J. R. Dorfman, Henk van Beijeren, and T. R. Kirkpatrick. *Contemporary Kinetic Theory of Matter*. Cambridge University Press, 2021.

## Appendix A: Numerical collision experiment

In this Appendix we describe the numerical collision experiment that aims to determine the scattering cross section of ratchet-shaped particles with a nonzero average rotation  $\Omega$  and fit to it the parameters  $r$  and  $\varepsilon$  of the toy model introduced in Sec. II. To do this, we initialize two particles with the sawblade shape presented in Fig. 2, characterized by the inner and outer radius  $R_{\text{inner}}$  and  $R_{\text{outer}}$ , initial rotation angles  $\psi_{1,2}^{(0)}$ , and angular velocities  $\omega_{1,2}$ . In the polar coordinate system centered on a given particle, the boundary radius of that particle is given by the formula

$$r_{1,2}(\phi) = R_{\text{inner}} + (R_{\text{outer}} - R_{\text{inner}}) \cdot \text{mod}(3\psi_{1,2}(\phi)/2\pi, 1), \quad (\text{A1})$$

where the phases  $\psi_{1,2}$  evolve in time as

$$\psi_{1,2}(\phi) = \phi - \psi_{1,2}^{(0)} - \omega_{1,2}t. \quad (\text{A2})$$

Furthermore, the centers of mass of the two particles are displaced by the distance  $b$  along the  $\mathbf{y}$  direction, and they perform uniform motion with velocities  $\mathbf{v}_{1,2}$  given by  $\mathbf{v}_2 = \frac{1}{2}g\hat{\mathbf{x}} = -\mathbf{v}_1$ , where  $g$  is the magnitude of the relative velocity. For reference, see Fig. 6. A single simulation is initialized with random initial phases  $\psi_{1,2}^{(0)}$  drawn from a uniform distribution  $\psi_{1,2}^{(0)} \in (0, 2\pi)$ , an impact parameter  $b$  drawn from a uniform distribution  $b \in (-R_{\text{outer}}, R_{\text{outer}})$ , and the relative velocity  $g$  and rotation frequencies  $\omega_{1,2}$  sampled according to

$$P(\omega_{1,2}, g) \sim g \exp\left(-\frac{\frac{1}{2}mg^2 + \sigma m R_{\text{outer}}^2 (\omega_{1,2} - \Omega)^2}{2k_b T}\right), \quad (\text{A3})$$

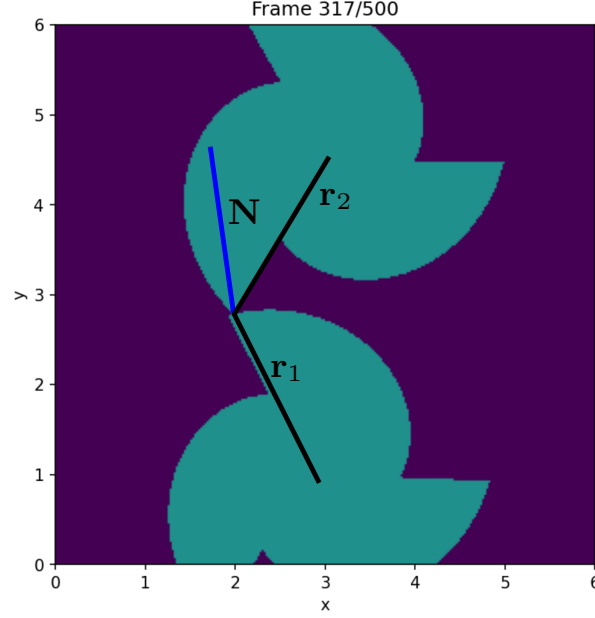


FIG. 6: Snapshot of ratchet-shaped particles colliding, showing the normal vector  $\mathbf{N}$  and the vectors  $\mathbf{r}_{1,2}$  that give the distance of the collision point from the respective ratchet centers. Here  $R_{\text{inner}} = 1.0$ ,  $R_{\text{outer}} = 2.0$ ,  $b = 3.5$ .

where  $\sigma$  is a dimensionless number such that the particle's moment of inertia is given by

$$I = \sigma m R_{\text{outer}}^2. \quad (\text{A4})$$

We consider only the case where the particles move towards each other. The evolution of the particles' shapes according to Eq. (A1) continues until the particles collide (see Figure 6), after which we compute the postcollisional velocities which allow us to extract the scattering angle. In order to compute the postcollisional velocities, we assume that the particles are perfectly smooth, which means that only the normal total relative velocity  $\mathbf{v}_{\text{rel}}$  of the particle is flipped, keeping the tangential one unchanged, i.e.

$$\mathbf{N} \cdot \mathbf{v}'_{\text{rel}} = -\mathbf{N} \cdot \mathbf{v}_{\text{rel}}, \quad \hat{\mathbf{z}} \cdot (\mathbf{N} \times \mathbf{v}'_{\text{rel}}) = \hat{\mathbf{z}} \cdot (\mathbf{N} \times \mathbf{v}_{\text{rel}}). \quad (\text{A5a})$$

The total relative velocity  $\mathbf{v}_{\text{rel}}$  is given by

$$\mathbf{v}_{\text{rel}} = \mathbf{v}_1 - \mathbf{v}_2 + \hat{\mathbf{z}} \times \mathbf{r}_1 \omega_1 - \hat{\mathbf{z}} \times \mathbf{r}_2 \omega_2, \quad (\text{A5b})$$

where  $\mathbf{r}_{1,2}$  is the distance vector of the collision point from the respective particles. From (A5), the outgoing linear velocities can be computed to be

$$\mathbf{v}'_{1,2} = \mathbf{v}_{1,2} \mp \mathbf{N} \frac{\mathbf{N} \cdot \mathbf{v}_{\text{rel}}}{1/m + \frac{\ell_1^2 + \ell_2^2}{2I}}, \quad (\text{A6})$$

where

$$\ell_{1,2} = \mathbf{N} \cdot \hat{\mathbf{z}} \times \mathbf{r}_{1,2} \quad (\text{A7})$$

In order to compute the normal vector  $\mathbf{N}$  we select the ratchet whose collision point is not at one of its pointy ends, as there  $\mathbf{N}$  becomes ambiguous. It follows from (A1) that

$$\mathbf{N}_{\text{unnorm}} = \pm \left[ \hat{\mathbf{r}}_{1,2} - \frac{\partial_{\phi} r_{1,2}(\phi)}{r_{1,2}(\phi)} \hat{\phi} \right]. \quad (\text{A8})$$

After  $\mathbf{N}_{\text{unnorm}}$  has been extracted, it is converted to Cartesian components and normalized to obtain  $\mathbf{N}$ . Through  $\mathbf{v}'_{1,2}$  we obtain the scattering angle  $\chi$ . Then, we store the scattering angle  $\chi$  for all trials where there is a collision for

all the impact parameters  $b$ . Dividing the full range of scattering angles into bins  $B_n$  with width  $\Delta\chi$ , the histogram of this collision can then be related to  $P(\chi|b)$  as

$$\frac{P(\chi \in B_n|b)}{\Delta\chi} \approx P(\chi|b) \quad , \quad (\text{A9})$$

with  $P(\chi \in B_n|b)$  representing the number of the trials that end up in  $B_n$  divided by the total number of scattering events for an impact parameter  $b$ . Then the differential cross section is calculated as

$$\frac{\partial\sigma_{\text{ratchet}}(\chi)}{\partial\chi} = \int db P(\chi|b) \quad . \quad (\text{A10})$$

(A10) is evaluated with a Riemann sum of  $b$  values that pass through the domain given by

$$-R_{\text{outer}} \leq b \leq R_{\text{outer}} \quad , \quad (\text{A11})$$

which is where ratchet collisions are theoretically possible. The differential cross section based on hard disks with chiral effective radii is given by

$$\begin{aligned} \frac{\partial\sigma_\varepsilon(\chi)}{\partial\chi} &= r(1 + \varepsilon) \sin(\chi/2) \quad 0 < \chi < \pi, \\ \frac{\partial\sigma_\varepsilon(\chi)}{\partial\chi} &= r(1 - \varepsilon) \sin(\chi/2), \quad \pi < \chi < 2\pi. \end{aligned}$$

We fit  $\varepsilon$  and  $r$  with the least squares method in order to best capture the differential cross section of the ratchet collision experiment with the chiral effective radius, which leads to the histogram shown in Fig. 3.

### Appendix B: $H$ -theorem

To show that  $H$ -theorem holds, it is helpful to write the collision integral as

$$C[f(\mathbf{v}_1)] = \iiint d\mathbf{v}_2 d\mathbf{v}'_2 d\mathbf{v}'_1 (W(\mathbf{v}_1, \mathbf{v}_2|\mathbf{v}'_1, \mathbf{v}'_2) f(\mathbf{v}'_1) f(\mathbf{v}'_2) - W(\mathbf{v}'_1, \mathbf{v}'_2|\mathbf{v}_1, \mathbf{v}_2) f(\mathbf{v}_1) f(\mathbf{v}_2)), \quad (\text{B1})$$

with the transition probability  $W(\mathbf{v}'_1, \mathbf{v}'_2|\mathbf{v}_1, \mathbf{v}_2)$  given by

$$W(\mathbf{v}'_1, \mathbf{v}'_2|\mathbf{v}_1, \mathbf{v}_2) = |\mathbf{g}| \sum_{\pm} \pm \frac{d(1 \pm \varepsilon)}{2} \int_0^{\pm\pi} d\chi \sin\left(\frac{\chi}{2}\right) \delta^{(2)}[\mathbf{v}'_1 - \mathbf{v}'_1(\mathbf{v}_1, \mathbf{v}_2, \chi)] \delta^{(2)}[\mathbf{v}'_2 - \mathbf{v}'_2(\mathbf{v}_1, \mathbf{v}_2, \chi)], \quad (\text{B2})$$

where the primed velocities are equal to

$$\mathbf{v}'_{1,2}(\mathbf{v}_1, \mathbf{v}_2, \chi) = \frac{\mathbf{v}_1 + \mathbf{v}_2}{2} \pm \mathbf{R}(\chi) \cdot \frac{\mathbf{v}_1 - \mathbf{v}_2}{2}, \quad (\text{B3})$$

as we infer from Eq. (2).  $H$ -theorem is typically derived by utilizing microscopic reversibility [44, 50]. However, the chirality of the collisions in Fig. 1 means that  $W$  is invariant under neither parity nor time-reversal:

$$W(\mathbf{v}'_1, \mathbf{v}'_2|\mathbf{v}_1, \mathbf{v}_2) \neq W(\mathbf{v}_1, \mathbf{v}_2|\mathbf{v}'_1, \mathbf{v}'_2). \quad (\text{B4})$$

Despite this, we can still prove the  $H$ -theorem

$$\frac{\partial H}{\partial t} \leq 0, \quad (\text{B5})$$

where the  $H$ -functional is given by

$$H = \iint d\mathbf{r} d\mathbf{v}_1 f(\mathbf{v}_1) \log(f(\mathbf{v}_1)) \quad . \quad (\text{B6})$$

To prove that (B5) holds, let us write

$$\frac{\partial H}{\partial t} = \int d\mathbf{r} Q \quad . \quad (\text{B7})$$

It follows from (6) that

$$Q = \int \cdots \int d\mathbf{v}'_1 d\mathbf{v}'_2 d\mathbf{v}_1 d\mathbf{v}_2 \log(f(\mathbf{v}_1)) (W(\mathbf{v}_1, \mathbf{v}_2 | \mathbf{v}'_1, \mathbf{v}'_2) f(\mathbf{v}'_1) f(\mathbf{v}'_2) - W(\mathbf{v}'_1, \mathbf{v}'_2 | \mathbf{v}_1, \mathbf{v}_2) f(\mathbf{v}_1) f(\mathbf{v}_2)). \quad (\text{B8})$$

Since the velocities in (B8) are dummy variables, it holds that

$$Q = \frac{1}{2} \int \cdots \int d\mathbf{v}'_1 d\mathbf{v}'_2 d\mathbf{v}_1 d\mathbf{v}_2 \log\left(\frac{f(\mathbf{v}'_1) f(\mathbf{v}'_2)}{f(\mathbf{v}_1) f(\mathbf{v}_2)}\right) W(\mathbf{v}_1, \mathbf{v}_2 | \mathbf{v}'_1, \mathbf{v}'_2) f(\mathbf{v}'_1) f(\mathbf{v}'_2). \quad (\text{B9})$$

Using (B2), we can calculate

$$\int d^2 v'_1 d^2 v'_2 W(\mathbf{v}'_1, \mathbf{v}'_2 | \mathbf{v}_1, \mathbf{v}_2) = 2d|\mathbf{g}|, \quad \int d^2 v_1 d^2 v_2 W(\mathbf{v}'_1, \mathbf{v}'_2 | \mathbf{v}_1, \mathbf{v}_2) = 2d|\mathbf{g}'|. \quad (\text{B10})$$

From (1) we learn that

$$|\mathbf{g}| = |\mathbf{g}'|. \quad (\text{B11})$$

It thus follows that

$$\int \cdots \int d\mathbf{v}'_1 d\mathbf{v}'_2 d\mathbf{v}_1 d\mathbf{v}_2 W(\mathbf{v}'_1, \mathbf{v}'_2 | \mathbf{v}_1, \mathbf{v}_2) f(\mathbf{v}'_1) f(\mathbf{v}'_2) = \int \cdots \int d\mathbf{v}'_1 d\mathbf{v}'_2 d\mathbf{v}_1 d\mathbf{v}_2 W(\mathbf{v}'_1, \mathbf{v}'_2 | \mathbf{v}_1, \mathbf{v}_2) f(\mathbf{v}_1) f(\mathbf{v}_2), \quad (\text{B12})$$

which can be rewritten as

$$\int \cdots \int d\mathbf{v}'_1 d\mathbf{v}'_2 d\mathbf{v}_1 d\mathbf{v}_2 W(\mathbf{v}'_1, \mathbf{v}'_2 | \mathbf{v}_1, \mathbf{v}_2) f(\mathbf{v}_1) f(\mathbf{v}_2) \left( \frac{f(\mathbf{v}'_1) f(\mathbf{v}'_2)}{f(\mathbf{v}_1) f(\mathbf{v}_2)} - 1 \right) = 0. \quad (\text{B13})$$

Using (B13), (B9) can be written as

$$Q = \frac{1}{2} \int \cdots \int d\mathbf{v}'_1 d\mathbf{v}'_2 d\mathbf{v}_1 d\mathbf{v}_2 \left[ \log\left(\frac{f(\mathbf{v}'_1) f(\mathbf{v}'_2)}{f(\mathbf{v}_1) f(\mathbf{v}_2)}\right) - \frac{f(\mathbf{v}'_1) f(\mathbf{v}'_2)}{f(\mathbf{v}_1) f(\mathbf{v}_2)} + 1 \right] W(\mathbf{v}'_1, \mathbf{v}'_2 | \mathbf{v}_1, \mathbf{v}_2) f(\mathbf{v}_1) f(\mathbf{v}_2). \quad (\text{B14})$$

Since it holds that [51]

$$\log(x) - x + 1 \leq 0, \quad x \geq 0 \quad (\text{B15})$$

it follows that

$$Q \leq 0, \quad (\text{B16})$$

so that (B5) is proven.

### Appendix C: Sonine polynomial expansion

In this Appendix we explain how to solve the linearized Boltzmann equation (11) for  $\Phi$  and thereby extract transport viscosity and thermal conductivity. Strictly speaking, the solution to (11) is not unique since  $C^{(1)}$  has a kernel spanned by the functions 1,  $c_i$  and  $\mathbf{c}^2$  (because collisions conserve particle number, linear momentum and kinetic energy), but as is customary, we make  $\Phi$  unique by defining the inner product in the space of complex functions

$$(\Phi, \Psi) = \int d\mathbf{v}_1 f_0(\mathbf{v}_1) \Phi(\mathbf{v}_1) \Psi(\mathbf{v}_1) \quad (\text{C1})$$

and demanding that

$$(\Phi, 1) = (\Phi, c_i) = (\Phi, \mathbf{c}^2) = 0. \quad (\text{C2})$$

The left-hand side of the Boltzmann equation (11) reads explicitly [52]:

$$\mathcal{L}[f_0] = f_0(\mathbf{v}, \mathbf{x}, t) \left[ \frac{m}{2k_b T} (c_i c_j - \frac{1}{2} \delta_{ij} c^2) (\partial_i u_j + \partial_j u_i) + \left( \frac{m c^2}{2k_b T} - 2 \right) c_i \partial_i \log T \right], \quad (\text{C3})$$

where  $\mathbf{c} \equiv \mathbf{v} - \mathbf{u}(\mathbf{x}, t)$  is called the peculiar velocity and we used the Einstein summation convention. From (C3) it follows that the solution has the form

$$\Phi = \sum_{(e,o)} \left( -\frac{1}{n} \sqrt{\frac{2k_b T}{m}} \mathbf{A}^{(e,o)} \cdot \nabla \log T - \frac{2}{n} \mathbf{B}^{(e,o)} : \nabla \mathbf{u} \right), \quad (\text{C4})$$

where  $\mathbf{A}^{(e,o)}$  and  $\mathbf{B}^{(e,o)}$  are some functions of  $\mathbf{c}$  to be determined. The tensors labeled ( $e$ ) are parity even, while the ones labeled ( $o$ ) are parity odd. Defining  $C^{(1)}[\Psi] = -n^2 I^{(1)}[\Psi]$ , where for a general field  $\Psi$  we have

$$I^{(1)}[\Psi] = \frac{d}{2n^2} \sum_{\pm} \pm (1 \pm \varepsilon) \int_0^{\pm\pi} d\chi \sin(\chi/2) \int d\mathbf{v}_2 |\mathbf{g}| f_0(\mathbf{v}) f_0(\mathbf{v}_2) [\Psi(\mathbf{v}) + \Psi(\mathbf{v}_2) - \Psi(\mathbf{v}'_1) - \Psi(\mathbf{v}'_2)] , \quad (\text{C5})$$

we can write (11) as

$$(\mathbf{X}\mathbf{X} - \mathbf{1}X^2/2)f_0(\mathbf{v}) = n \sum_{(e,o)} I^{(1)}[\mathbf{B}^{(e,o)}], \quad (\text{C6a})$$

$$(X^2 - 2) \mathbf{X}f_0(\mathbf{v}) = n \sum_{(e,o)} I^{(1)}[\mathbf{A}^{(e,o)}], \quad (\text{C6b})$$

where we introduced the dimensionless velocity

$$\mathbf{X} = \sqrt{\frac{m}{2k_b T}} \mathbf{c}. \quad (\text{C7})$$

To solve (C6), we expand  $\mathbf{A}^{(e,o)}$  and  $\mathbf{B}^{(e,o)}$  in the basis of the Sonine polynomials  $S_n^{(m)}$ , also known as the generalized Laguerre polynomials. The Sonine polynomials satisfy the following identity involving the inner product in Eq. (C1):

$$(S_n^{(m)}, X^{2m} S_{n'}^{(m)}) = \delta_{nn'} \frac{(n+m)!}{n!}. \quad (\text{C8})$$

Our expansion reads

$$\mathbf{B}^{(e,o)} = \sum_{n=0}^N \mathfrak{b}_n^{(e,o)} \mathbf{b}_n^{(e,o)}, \quad \mathbf{b}_n^{(e,o)} = \mathbf{X}\mathbf{X} : \mathbf{T}^{(e,o)} S_n^{(2)}(X^2) \quad (\text{C9a})$$

and

$$\mathbf{A}^{(e,o)} = \sum_{n=1}^{N+1} \mathfrak{a}_n^{(e,o)} \mathbf{a}_n^{(e,o)}, \quad \mathbf{a}_n^{(e,o)} = \mathbf{X} \cdot \mathbf{P}^{(e,o)} S_n^{(1)}(X^2), \quad (\text{C9b})$$

where  $\mathfrak{b}_n^{(e,o)}$  and  $\mathfrak{a}_n^{(e,o)}$  are constants and we introduced the tensors

$$P_{ij}^{(e)} = \delta_{ij}, \quad P_{ij}^{(o)} = \epsilon_{ij}, \quad T_{ijkl}^{(e)} = \frac{1}{2} (\delta_{ik}\delta_{jl} + \delta_{jk}\delta_{il} - \delta_{ij}\delta_{kl}), \quad T_{ijkl}^{(o)} = \frac{1}{2} (\delta_{ik}\epsilon_{jl} + \delta_{jl}\epsilon_{ik}). \quad (\text{C10})$$

The tensors  $\mathbf{P}^{(e,o)}$  are the only two-component tensors consistent with isotropy in two dimensions, and likewise  $T^{(e,o)}$  are the only isotropic four-component tensors symmetric and traceless in the last two indices, related to the fact that only the traceless part is nonzero on the left hand side of (C6a). We excluded  $S_0^{(1)}(X^2)$  in the sum of (C9b) to satisfy (C2). Using Eq. (C8), we derive from (C6a) the relations

$$\sum_{m=0}^N \int d\mathbf{v} \mathbf{b}_m^{(e)} : I^{(1)} [\mathfrak{b}_m^{(e)} \mathbf{b}_m^{(e)} + \mathfrak{b}_m^{(o)} \mathbf{b}_m^{(o)}] \equiv \mathbf{b}_N \cdot \mathfrak{b}^{(e)} + \mathbf{b}'_N \cdot \mathfrak{b}^{(o)} = \frac{1}{2} \delta_{n0}, \quad (\text{C11a})$$

$$\sum_{m=0}^N \int d\mathbf{v} \mathbf{b}_m^{(o)} : I^{(1)} [\mathfrak{b}_m^{(e)} \mathbf{b}_m^{(e)} + \mathfrak{b}_m^{(o)} \mathbf{b}_m^{(o)}] \equiv \mathbf{b}_N^* \cdot \mathfrak{b}^{(e)} + \mathbf{b}'_N \cdot \mathfrak{b}^{(o)} = 0, \quad (\text{C11b})$$

whereas we find from (C6b) the relations

$$\sum_{m=1}^{N+1} \int d\mathbf{v} \mathbf{a}_n^{(e)} \cdot I^{(1)} \left[ \mathfrak{a}_m^{(e)} \mathbf{a}_m^{(e)} + \mathfrak{a}_m^{(o)} \mathbf{a}_m^{(o)} \right] \equiv \mathbf{a}_N \cdot \mathfrak{a}^{(e)} + \mathbf{a}'_N \cdot \mathfrak{a}^{(o)} = 2\delta_{n0}, \quad (\text{C12a})$$

$$\sum_m^{N+1} \int d\mathbf{v} \mathbf{a}_n^{(o)} \cdot I^{(1)} \left[ \mathfrak{a}_m^{(e)} \mathbf{a}_m^{(e)} + \mathfrak{a}_{m=1}^{(o)} \mathbf{a}_m^{(o)} \right] \equiv \mathbf{a}_N^* \cdot \mathfrak{a}^{(e)} + \mathbf{a}'_N^* \cdot \mathfrak{a}^{(o)} = 0. \quad (\text{C12b})$$

The out-of-equilibrium stress tensor  $\sigma_{ij}$  and the heat current  $q_i$  are

$$\sigma_{ij} = (c_i c_j, \Phi) \quad , \quad q_i = \left( \frac{mc^2}{2} c_i, \Phi \right) \quad . \quad (\text{C13})$$

The transport coefficients enter into these currents as

$$\sigma_{ij} = -2 \sum_{(e,o)} \eta_{e,o} T_{ijkl}^{(e,o)} \partial_k u_l, \quad (\text{C14a})$$

$$q_i = - \sum_{(e,o)} \kappa_{e,o} P_{ij}^{(e,o)} \partial_j \log T, \quad (\text{C14b})$$

Therefore, we find the following formulae for the transport coefficients:

$$\eta_{e,o}^{(N)} = \mathfrak{b}_0^{(e,o)} k_b T \quad (\text{C15a})$$

$$\kappa_{e,o}^{(N)} = \mathfrak{a}_1^{(e,o)} \frac{(k_b T)^2}{m} \quad (\text{C15b})$$

From (C11) it follows that

$$\eta_e^{(N)} = \frac{1}{2} k_b T (\mathbf{b}_N + \mathbf{b}'_N (\mathbf{b}_N)^{-1} \mathbf{b}'_N)_{00}^{-1} \quad , \quad (\text{C16a})$$

$$\eta_o^{(N)} = \frac{1}{2} k_b T (\mathbf{b}'_N + \mathbf{b}_N (\mathbf{b}'_N)^{-1} \mathbf{b}_N)_{00}^{-1} \quad , \quad (\text{C16b})$$

where we used that

$$\mathbf{b}_N = \mathbf{b}'_N \quad , \quad \mathbf{b}'_N = -\mathbf{b}_N^* \quad . \quad (\text{C17a})$$

Similarly, we find from (C12) that

$$\kappa_e^{(N)} = \frac{2(k_b T)^2}{m} (\mathbf{a}_N + \mathbf{a}'_N (\mathbf{a}_N)^{-1} \mathbf{a}'_N)_{11}^{-1} \quad , \quad (\text{C18a})$$

$$\kappa_o^{(N)} = \frac{2(k_b T)^2}{m} (\mathbf{a}'_N + \mathbf{a}_N (\mathbf{a}'_N)^{-1} \mathbf{a}_N)_{11}^{-1} \quad , \quad (\text{C18b})$$

where we used that

$$\mathbf{a}_N = \mathbf{a}'_N \quad , \quad \mathbf{a}'_N = -\mathbf{a}_N^* \quad . \quad (\text{C19a})$$

Lastly, we have

$$N_e^{(N)}(\varepsilon) = \left( b_0 + \frac{(b'_0)^2}{b_0} \right) (\mathbf{b}_N + \mathbf{b}'_N (\mathbf{b}_N)^{-1} \mathbf{b}'_N)_{00}^{-1} \quad , \quad (\text{C20a})$$

$$N_o^{(N)}(\varepsilon) = \left( b'_0 + \frac{b_0^2}{b'_0} \right) (\mathbf{b}'_N + \mathbf{b}_N (\mathbf{b}'_N)^{-1} \mathbf{b}_N)_{00}^{-1} \quad , \quad (\text{C20b})$$

and

$$K_e^{(N)}(\varepsilon) = \left( a_1 + \frac{(a'_1)^2}{a_1} \right) (\mathbf{a}_N + \mathbf{a}'_N (\mathbf{a}_N)^{-1} \mathbf{a}'_N)_{11}^{-1} \quad , \quad (\text{C21a})$$

$$K_o^{(N)}(\varepsilon) = \left( a'_1 + \frac{a_1^2}{a'_1} \right) (\mathbf{a}'_N + \mathbf{a}_N (\mathbf{a}'_N)^{-1} \mathbf{a}_N)_{11}^{-1} \quad , \quad (\text{C21b})$$

which gives (13).

To better understand how the elements of the matrices in (C16) and (C18) are computed, let us explicitly work out  $b_0$  and  $b'_0$ , which allow for the determination of  $\eta_e^{(0)}$  and  $\eta_o^{(0)}$ . Using (C5), we find

$$b_0 = \frac{d}{\pi^2} \sqrt{\frac{k_b T}{2m}} \sum_{\pm} \pm(1 \pm \varepsilon) \cdot \int_0^{\pm\pi} d\chi \sin(\chi/2) \iint d\mathbf{X} d\mathbf{X}_2 |\mathbf{X} - \mathbf{X}_2| \exp(-X^2 - X_2^2) [\mathbf{X}\mathbf{X} + \mathbf{X}_2\mathbf{X}_2 - \mathbf{X}'_1\mathbf{X}'_1 - \mathbf{X}'_2\mathbf{X}'_2] : \mathbf{T}^{(e)} : \mathbf{X}\mathbf{X} , \quad (\text{C22a})$$

$$b'_0 = \frac{d}{\pi^2} \sqrt{\frac{k_b T}{2m}} \sum_{\pm} \pm(1 \pm \varepsilon) \cdot \int_0^{\pm\pi} d\chi \sin(\chi/2) \iint d\mathbf{X} d\mathbf{X}_2 |\mathbf{X} - \mathbf{X}_2| \exp(-X^2 - X_2^2) [\mathbf{X}\mathbf{X} + \mathbf{X}_2\mathbf{X}_2 - \mathbf{X}'_1\mathbf{X}'_1 - \mathbf{X}'_2\mathbf{X}'_2] : \mathbf{T}^{(o)} : \mathbf{X}\mathbf{X} . \quad (\text{C22b})$$

Momentum conservation during the collision allows us to parametrize the variables in (C22) as

$$\mathbf{X} = \mathbf{X}_G + \frac{1}{2}\mathbf{X}_g , \quad \mathbf{X}_2 = \mathbf{X}_G - \frac{1}{2}\mathbf{X}_g , \quad \mathbf{X}'_1 = \mathbf{X}_G + \frac{1}{2}\mathbf{X}'_g , \quad \mathbf{X}'_2 = \mathbf{X}_G - \frac{1}{2}\mathbf{X}'_g , \quad (\text{C23})$$

so that (C22) can be rewritten as

$$b_0 = \frac{d}{\pi^2} \sqrt{\frac{k_b T}{2m}} \sum_{\pm} \pm(1 \pm \varepsilon) \cdot \int_0^{\pm\pi} d\chi \sin(\chi/2) \iint d\mathbf{X}_G d\mathbf{X}_g |\mathbf{X}_g| \exp\left(-\frac{1}{2}X_g^2 - 2X_G^2\right) [\mathbf{X}\mathbf{X} + \mathbf{X}_2\mathbf{X}_2 - \mathbf{X}'_1\mathbf{X}'_1 - \mathbf{X}'_2\mathbf{X}'_2] : \mathbf{T}^{(e)} : \mathbf{X}\mathbf{X} , \quad (\text{C24a})$$

$$b'_0 = \frac{d}{\pi^2} \sqrt{\frac{k_b T}{2m}} \sum_{\pm} \pm(1 \pm \varepsilon) \cdot \int_0^{\pm\pi} d\chi \sin(\chi/2) \iint d\mathbf{X}_G d\mathbf{X}_g |\mathbf{X}_g| \exp\left(-\frac{1}{2}X_g^2 - 2X_G^2\right) [\mathbf{X}\mathbf{X} + \mathbf{X}_2\mathbf{X}_2 - \mathbf{X}'_1\mathbf{X}'_1 - \mathbf{X}'_2\mathbf{X}'_2] : \mathbf{T}^{(o)} : \mathbf{X}\mathbf{X} , \quad (\text{C24b})$$

From conservation of energy given by (1b), it follows that  $\mathbf{X}_g' = |\mathbf{X}_g|(\cos(\chi), \sin(\chi))$  when  $\mathbf{X}_g = |\mathbf{X}_g|(1, 0)$ , which for this integral we can assume without loss of generality. With this information, we can straightforwardly work out the integral of (C24), which yields

$$b_0 = d\sqrt{\frac{\pi k_b T}{m}} , \quad b'_0 = -\frac{d\epsilon}{4}\sqrt{\frac{\pi k_b T}{m}} , \quad (\text{C25})$$

from which the first line of (14) follows when plugged into (C16) for  $N = 0$ . A similar calculation allows us to arrive at

$$a_1 = d\sqrt{\frac{\pi k_b T}{m}} , \quad a'_1 = -\frac{d\epsilon}{4}\sqrt{\frac{\pi k_b T}{m}} , \quad (\text{C26})$$

which plugged into (C18) gives the second line of (14).

#### Appendix D: Nonequilibrium molecular dynamics

In this Appendix we describe the nonequilibrium molecular dynamics computations that we perform to verify (14). In the simulation, we consider a shear periodic box of hard disks which collide with the collision rule of Fig. 1. We turn on shear using the SLLOD algorithm [34, 46–48], which means that particles evolve according to

$$\begin{aligned} \dot{x}_i &= u_i + \gamma y_i , & \dot{y}_i &= v_i , \\ \dot{u}_i &= \frac{1}{m} \sum_{j \neq i} f_{ij}^x - \gamma v_i + \alpha u_i , & \dot{v}_i &= \sum_{j \neq i} f_{ij}^y + \alpha v_i , \end{aligned} \quad (\text{D1})$$

where  $\gamma$  is the shear rate and  $\mathbf{f}_{ij}$  is the force on particle  $i$  due to collisions with particle  $j$ . The coefficient  $\alpha$  is related to a thermostat mechanism introduced to prevent the system from heating up, which will be discussed shortly. We consider shear  $\gamma$  that acts with a constant magnitude during a single run, but its sign changes periodically, with the period long enough that the gas has enough time to thermalize. To extract viscosity, we compute

$$\eta = \left\langle \frac{\sigma_{xy}}{\gamma} \right\rangle, \quad \eta_o = \frac{1}{2} \left\langle \frac{\sigma_{xx} - \sigma_{yy}}{\gamma} \right\rangle, \quad (\text{D2})$$

where  $\langle \dots \rangle$  corresponds to an average over the run and  $\boldsymbol{\sigma}$  is the Irving-Kirkwood stress given by

$$\boldsymbol{\sigma} = -\frac{1}{A} \left[ \sum_i m \mathbf{v}_i \mathbf{v}_i + \frac{1}{2} \sum_{i \neq j} \mathbf{f}_{ij} \mathbf{r}_{ij} \right], \quad (\text{D3})$$

where  $A$  is the box area. Because of the simple hard disk nature of the collisions, the second term on the right hand side of (D3) reduces to

$$\frac{1}{2} \sum_{i \neq j} \mathbf{f}_{ij} \mathbf{r}_{ij} = m \sum_{n_c} \frac{\Delta \mathbf{v}_{n_c}}{\Delta t} \Delta \mathbf{x}_{n_c}, \quad (\text{D4})$$

where  $\Delta \mathbf{v}_{n_c}$  is the change of velocity of the colliding particles caused by the  $n_c$ th collision of a time step of the numerical simulation and  $\Delta t$  is the width of this time step. Note that because  $\mathbf{v}_{n_c} \perp \mathbf{x}_{n_c}$ , it holds that  $\boldsymbol{\sigma} = \boldsymbol{\sigma}^T$ , confirming that the chiral collisions considered in this work conserve angular momentum.

The shear induced by  $\gamma$  heats up the system, which is problematic because the transport coefficients we wish to compute depend on temperature. To remedy this, we use a thermostat that controls the temperature. In particular, we choose  $\alpha$  in (D1) in such a way that total momentum is conserved and the added kinetic energy due to shearing is canceled out, i.e.

$$\frac{1}{2} m \frac{\partial}{\partial t} \sum_i (u_i^2 + v_i^2) = -m \sum_i (\gamma v_i u_i + \alpha (u_i^2 + v_i^2)) = 0, \quad (\text{D5})$$

which requires that [46]

$$\alpha = \frac{\gamma \sum_i v_i u_i}{\sum_i (v_i^2 + u_i^2)}. \quad (\text{D6})$$

After cooling the system down with this thermostat, there is still a tiny amount of heating which adds up after a large number of time steps. To eliminate this residual heating effect, we additionally cool down the system by subtracting the mean velocity and rescaling the velocities. In Fig. 5, we compare the viscosities that follow from our numerical simulation for 5 different temperatures and  $\varepsilon = 0.5$ .